Formation and dissociation of Zn nanoclusters in MgO

van Huis, MA; van Veen, A; Schut, H; Kooi, BJ; De Hosson, JTM; Du, XS; Hibma, T; Fromknecht, R

Published in:
Nuclear Instruments & Methods in Physics Research Section B-Beam Interactions with Materials and Atoms

DOI:
10.1016/j.nimb.2003.11.065

Publication date:
2004

Available online at www.sciencedirect.com
SCIENCE DIRECT®
ELSEVIER
Nuclear Instruments and Methods in Physics Research B 216 (2004) 390–395
NIM B
Beam Interactions with Materials & Atoms
www.elsevier.com/locate/nimb

Formation and dissociation of Zn nanoclusters in MgO

M.A. van Huis [a,*], A. van Veen [a], H. Schut [a], B.J. Kooi [b], J.Th.M. De Hosson [b], X.S. Du [b], T. Hibma [b], R. Fromknecht [c]

[a] *Interfaculty Reactor Institute, Delft University of Technology, Mekelweg 15, 2629 JB Delft, The Netherlands*
[b] *Materials Science Center, University of Groningen, Nijenborgh 4, 9749 AG Groningen, The Netherlands*
[c] *Institüt für Festkörperphysik, Forschungszentrum Karlsruhe, Hermann-von-Helmholtz-Platz 1, 76344 Eggenstein-Leopoldshafen, Germany*

Abstract

Zinc nanoclusters were created in MgO by implantation of 1×10^{17} Zn ions cm^{-2} at an energy of 140 keV and subsequent thermal annealing. The defect evolution was investigated by means of optical absorption spectroscopy, Rutherford backscattering spectrometry and channeling, Doppler broadening positron beam analysis, and with cross-sectional transmission electron microscopy (XTEM). After annealing at 1150 K, an optical absorption band appears due to plasmon resonance. TEM investigations confirm that metallic Zn nanoclusters with sizes of 5–10 nm are formed at this temperature. The nanoclusters have the hcp Zn crystal structure and the *c*-axis is aligned with one of the cubic MgO axes, i.e. MgO(0 0 1)||Zn(0 0 0 1). The nanoclusters dissociate during annealing at 1550 K. At this temperature, the Zn is dissolved and diffuses into the MgO matrix.

PACS: 61.46.+w; 61.72.Ji; 68.55.Ln; 78.70.B
Keywords: Ion implantation; Nanoclusters; Structural properties; Defects

1. Introduction

Metal and semiconductor nanoclusters embedded in glasses are composite materials with promising optical properties. Semiconductor ZnO nanoclusters are known for their photoluminescence [1–3] and also exhibit strong third-order optical non-linearity [4]. Metallic Zn nanoclusters have optical absorption due to Mie plasmon resonance [5] and have a paramagnetic susceptibility that depends on the nanocluster size [6]. In this work, it is attempted to create ZnO nanoclusters in MgO by Zn ion implantation and internal oxidation by thermal annealing in an oxidising environment. Earlier investigations include Zn ion implantation in silica [7,8] and in sapphire Al_2O_3 [9]. The defect evolution during the annealing treatment is monitored with four complementary techniques that are discussed below.

2. Experimental

In order to create nanoclusters, monocrystalline MgO(0 0 1) samples were implanted with doses of

* Corresponding author. Tel.: +31-15-2781612; fax: +31-15-2786422.
E-mail address: vanhuis@iri.tudelft.nl (M.A. van Huis).

0168-583X/$ - see front matter © 2003 Elsevier B.V. All rights reserved.
doi:10.1016/j.nimb.2003.11.065

1×10^{17} Zn ions cm^{-2} at an energy of 140 keV. This corresponds to a peak concentration of implanted Zn of 20 at.%. After ion implantation, isochronal annealing was performed in ambient air at temperatures up to 1550 K in steps of 200 K, during periods of 0.5 h. After ion implantation and after each annealing step, the defect evolution in the sample was monitored using optical absorption spectroscopy (OAS), Doppler broadening positron beam analysis (PBA), Rutherford backscattering and channeling (RBS-C). Optical absorption spectroscopy was used to detect metal nanocluster formation due to Mie surface plasmon resonance [10,11]. Strictly speaking, the conduction electrons of Zn cannot be considered as free electrons, which is required for application of the Drude–Lorentz–Sommerfeld model [10]. However, the interband transitions in Zn result in plasmon behaviour [12] and we will apply the Mie theory as an approximation. Positron beam analysis (PBA) [13] was used to follow the defect evolution. Positrons that are implanted in a material annihilate with electrons, giving two γ quanta per annihilation with an energy of 511 keV each. The energy of the photons is measured using an energy-sensitive detector and accumulated in a multi-channel analyser. The non-zero momentum of the electrons leads to a Doppler broadening of the 511 keV annihilation peak. The so-called S (shape) parameter is derived from the 511 keV peak and indicates the contribution of valence and conduction electrons to the annihilation spectrum [13]. Ion implantation leads to the formation of vacancies where positrons are effectively trapped and mainly annihilate with valence electrons. Hence, the S parameter is a very sensitive indicator of ion implantation damage. PBA is also a depth-sensitive technique; the probe depth in the sample can be varied by varying the implantation energy of the positron beam. In this work, a mono-energetic positron beam with a variable energy of 0–30 keV was used, allowing detection up to 2 μm in depth.

One sample was also examined by means of cross-sectional transmission electron microscopy (XTEM) after the 1150 K annealing step. The microscope was a JEOL 4000 EX/II operating at 400 kV with a point-to-point resolution of 0.17 nm. The specimen preparation is discussed elsewhere [14]. RBS-C was used to detect damage recovery in the MgO and migration of implanted Zn atoms. The samples that were measured with RBS-C were implanted under different implantation conditions, because these samples were produced as part of an older experimental program. Here a lower total dose of 1.4×10^{16} Zn ions cm^{-2} was implanted at energies ranging from 35 to 280 keV in order to create a flat Zn implantation profile. The RBS setup consists of a beam of 2.0 MeV He ions in combination with a 3-axes goniometer. Using these four complementary techniques, a good understanding is obtained of the defect evolution.

3. Results and discussion

3.1. Optical absorption spectroscopy and RBS-C

Fig. 1 shows the optical absorption spectra after implantation of 1×10^{17} Zn ions cm^{-2} and after various annealing steps. The presence of Zn nanoclusters results in optical absorption due to Mie

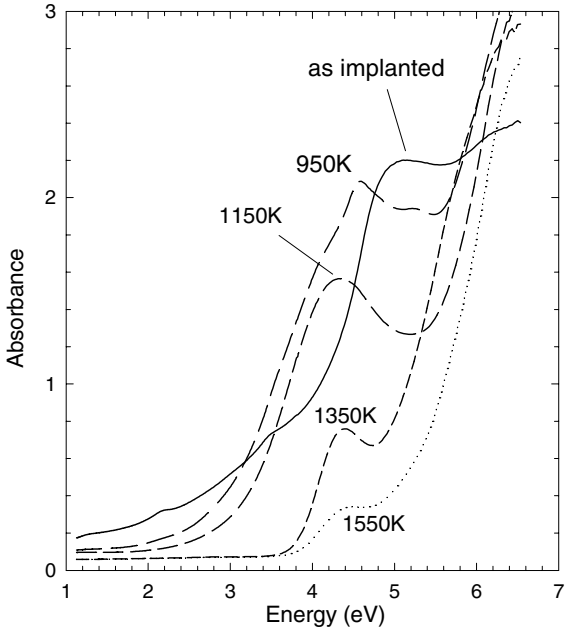

Fig. 1. Optical absorption spectra of MgO as-implanted with 1×10^{17} Zn ions cm^{-2} and after annealing at various temperatures.

plasmon resonance [10]. Unfortunately, the wavelength-dependent optical constants of MgO and Zn [11,12] are such that the Mie plasmon resonance peak interferes with the F-centers of MgO (O vacancies) at a photon energy of 4.9 eV and with Fe^{3+} impurity centers at 4.4 eV [15]. After annealing at 950 K, it is clear that the Fe^{3+} impurity peak is superimposed on a broader absorption peak. After annealing at 1150 K this broad absorption peak, which is due to Mie plasmon resonance, is well pronounced and has a centroid at a photon energy of 4.2 eV.

Results that have been published in the literature show that ZnO nanoclusters have an absorption edge at 3.3 eV at room temperature [3,4]. Comparing the absorption curves in Fig. 1 with the absorption curves of ZnO nanoclusters in the literature, it can be concluded that there is no evidence of ZnO nanocluster formation. The TEM analysis discussed below shows that after annealing at 1150 K, the clusters are made up of metallic Zn rather than semiconductor ZnO. Therefore, both the optical and TEM results show that the clusters are metallic at least up to a temperature of 1150 K. The absorption peak at 4.2 eV decreases upon annealing at 1350 K and almost vanishes after annealing at 1550 K, suggesting shrinkage and dissociation of the Zn nanoclusters. This implies that the Zn has dissolved in the MgO matrix, which was confirmed by RBS-C measurements that were performed on a MgO sample implanted with Zn ions under slightly different ion implantation conditions. Here a total of 1.4×10^{16} Zn ions cm^{-2} were implanted at energies varying between 35 and 280 keV in order to create a flat Zn implantation profile. These samples were subjected to the same annealing treatments as the high-dose 140 keV Zn implanted samples. The RBS-C shows that the Zn atoms diffuse into the MgO matrix at temperatures of 1550 K or higher. Of course, the Zn ion implantation conditions of the RBS-C samples are somewhat different, but it is not likely that this affects the solution energy (temperature) of Zn in MgO.

3.2. Positron beam analysis

Doppler broadening positron beam analysis (PBA) is a very sensitive technique to monitor ion implantation damage; a high S parameter indicates open volume defects. Fig. 2 shows the S parameter as a function of the positron implantation energy for the sample after implantation of 1.0×10^{17} Zn ions cm^{-2} and after annealing at various temperatures. The depth resolution is limited (in particular at higher positron implantation energies) due to the broadness of the positron implantation profile and positron diffusion processes. The positron implantation energy corresponds to an average depth that is indicated at the top of the figure. In order to facilitate the discussion, four layers are indicated in Fig. 2. The top layer I contains mainly damages created by the ion implantation, layer II implanted ions, and layer III a 'tail' of ion implantation defects caused by channelling effects (layer IV is the MgO bulk). Comparing the curve of the as-implanted sample with that of reference MgO, it is clear that the S parameter rises in layers I and II. After annealing at 1150 K, there are two peaks in the S parameter corresponding to open volume defects created by

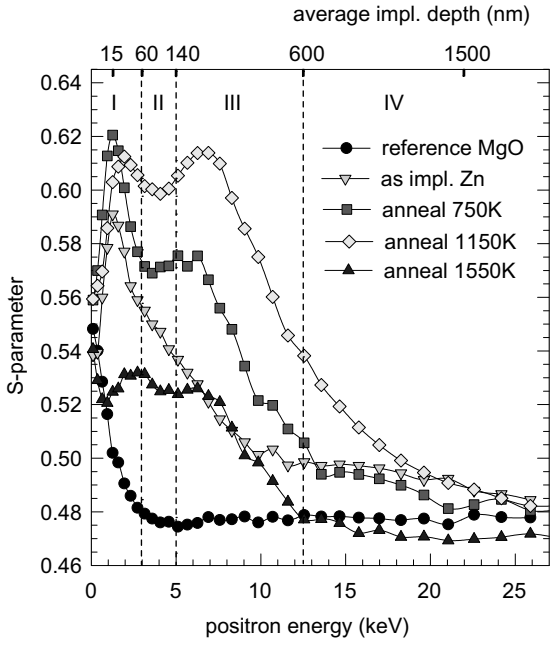

Fig. 2. S parameter as a function of positron implantation energy, after ion implantation of 1×10^{17} Zn ions cm^{-2} and after annealing at various temperatures. The average positron implantation depth is indicated at the top of the figure.

agglomeration of vacancies. Of course, vacancies have also been created in the ion implantation range (layer II), but here the implanted Zn ions have recombined with these vacancies. So in layer II the S parameter is lower because there are less open volume defects. After annealing at 1350 and 1550 K, the S parameter decreases in layers I, II and III, indicating recovery of ion implantation damage. Furthermore, the S parameter in the MgO bulk (layer IV) is lower than that of unimplanted MgO after annealing at 1550 K. This unusual observation suggests that the MgO bulk has changed, which is in agreement with the RBS results discussed above showing that Zn dissolves into MgO upon annealing at 1550 K.

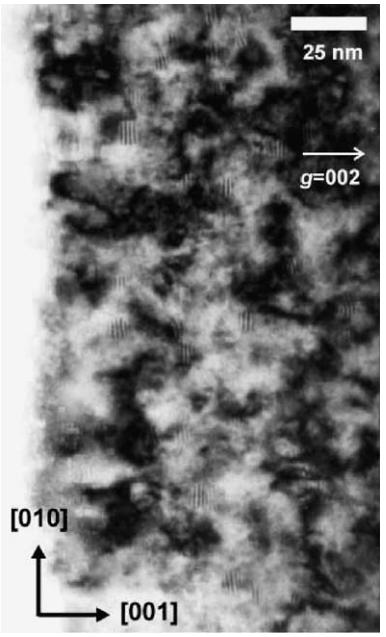

Fig. 3. Bright-field TEM image showing moiré fringes belonging to Zn nanoclusters created by implantation of 1×10^{17} Zn ions cm^{-2} and subsequent annealing at 1150 K. Only those clusters are visible that have the c-axis aligned with the MgO[0 0 1] axis.

3.3. XTEM

The evolution of ion implantation defects always starts with recombination and dissociation of the smallest defects and evolution into larger defects (vacancy cluster agglomeration, formation of nanoclusters and dislocation loops). Above a certain temperature, this process is followed by the shrinkage and dissociation of larger defects. From the optical and PBA results, the sample annealed at 1150 K was chosen as the most interesting point for XTEM analysis. Fig. 3 shows a bright-field XTEM image of this sample. The Zn clusters can be easily observed from the moiré fringes and are about 5–10 nm in size. Fig. 4(a) shows a high-resolution image of a Zn nanocluster. From Fig. 3, it appears that clusters exhibit the same orientation and that only translational moiré fringes are

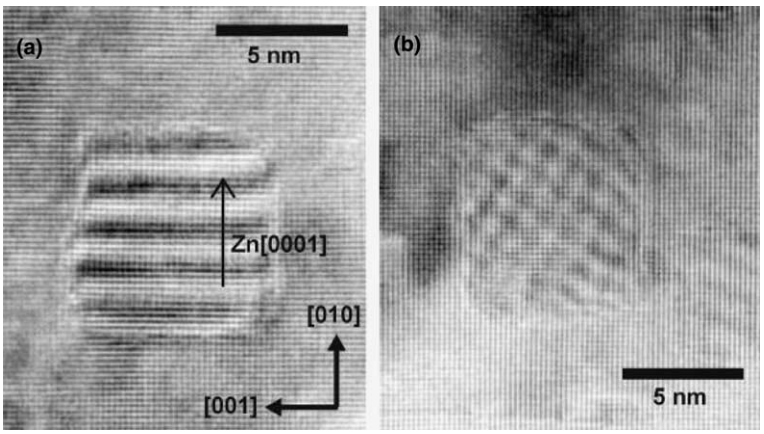

Fig. 4. High-resolution TEM images showing a Zn nanocluster (a) with translational moiré fringes along the MgO[0 1 0] axis and (b) with general moiré fringes.

found. However, when selecting other diffraction conditions or when operating in high-resolution mode, other types of moiré fringes were observed as well. Fig. 4(b) shows a high-resolution image of a Zn nanocluster with general moiré fringes. In Fig. 4(a) the translational moiré fringes run in the [0 1 0] direction. Simultaneously though, clusters can be found that have the same moiré fringes running in the [0 0 1] direction (with the clusters close to each other, in the same area, observed under the same diffraction conditions). From these observations and the spacing of the moiré fringes discussed below, it is most likely that the c-axis of hexagonal Zn is aligned with one of the cubical MgO[0 0 1] axes. The lattice spacing of Zn crystals in the [0 1 0] direction of the host can be determined from the relationship between d_{fringes} observed in Fig. 4(a) and lattice spacings.

$$\frac{1}{d_{\text{fringes}}} = \left| \frac{1}{d_{\text{MgO}}} - \frac{1}{d_{\text{Zn}}} \right|. \quad (1)$$

MgO has a lattice parameter of 4.212 Å so that $d_{\text{MgO}(0\,0\,2)} = 2.106$ Å. There are 4 moiré fringes in 29 MgO lattice spacings and application of Eq. (1) then yields $d_{\text{Zn}} = 2.44$ Å. The lattice parameters of hexagonal zinc are $a = 2.67$ Å and $c = 4.95$ Å [16]. Therefore, $d_{\text{Zn}(0\,0\,0\,2)} = 2.47$ Å, which corresponds very well with the d_{Zn} calculated from the moiré fringes. So the Zn nanoclusters have the usual hcp crystal structure and the c-axis is aligned with one of the cubic MgO axes: MgO(0 0 1)||Zn(0 0 0 1). Considering Fig. 4(a), the translational moiré fringes will run in the [0 1 0] direction when the c-axis is aligned with the MgO[0 1 0] axis and in the [0 0 1] direction when the c-axis is aligned with the MgO[0 0 1] axis. The rotational moiré observed in Fig. 4(b) can occur when the c-axis is perpendicular to the image in Fig. 4, i.e. in the [1 0 0] direction. The MgO||Zn alignment within the basal plane (perpendicular to the c-axis) is not clear from the TEM results.

High-resolution X-ray diffraction performed on the same sample (implanted with 1×10^{17} Zn ions cm^{-2} and annealed at 1150 K) has confirmed that the c-axis of Zn is aligned with the MgO[0 0 1] axis. More XRD experiments and analysis are required to determine the Zn-MgO orientation relationship within the basal plane of Zn.

4. Conclusions

Metallic zinc nanoclusters were created in MgO by means of ion implantation and subsequent annealing. An optical absorption peak appears at 4.2 eV after annealing at 1150 K caused by Mie plasmon resonance in metallic Zn nanoclusters. TEM investigations that were performed after annealing at 1150 K show that the nanoclusters have sizes of 5–10 nm and have the usual hcp Zn crystal structure. The c-axis of Zn is aligned with the cubic MgO axes, MgO(0 0 1)||Zn(0 0 0 1). Optical, RBS-C and PBA results show that the nanoclusters dissociate during annealing at a temperature of 1550 K; the Zn is dissolved and diffuses into the MgO matrix. No evidence was found for the presence of ZnO nanoclusters. For future attempts to create ZnO nanoclusters, it is recommended to use co-implantation of the same dose of Zn and O ions instead of relying on internal oxidation.

References

[1] E.M. Wong, P.C. Searson, Appl. Phys. Lett. 74 (1999) 2939.
[2] S. Mahamuni, K. Borgohain, B.S. Bendre, V.J. Leppert, S.H. Risbud, J. Appl. Phys. 85 (1999) 2861.
[3] P. Zu, Z.K. Tang, G.K.L. Wong, M. Kawasaki, A. Ohtomo, H. Koinuma, Y. Segawa, Solid State Commun. 103 (1997) 459.
[4] W. Zhang, H. Wang, K.S. Wong, Z.K. Tang, G.K.L. Wong, R. Jain, Appl. Phys. Lett. 75 (1999) 3321.
[5] S. Nakao, S. Utsunomiya, K. Sun, L.M. Wang, Y. Miyagawa, S. Miyagawa, presented at the 17th Int. Conf. on the Application of Accelerators in Research and Industry (CAARI 2002), Denton, TX, USA, 2002.
[6] S. Pasche, J.-P. Borel, Z. Phys. D 12 (1989) 401.
[7] Y.X. Liu, Y.C. Liu, D.Z. Shen, G.Z. Zhong, X.W. Fan, X.G. Kong, R. Mu, D.O. Henderson, Solid State Commun. 121 (2002) 531.
[8] J. Chen, R. Mu, A. Ueda, M.H. Wu, Y.-S. Tung, Z. Gu, D.O. Henderson, C.W. White, J.D. Budai, R.A. Zuhr, J. Vac. Sci. Technol. A 16 (1998) 1409.
[9] C.W. White, A. Meldrum, E. Sonder, J.D. Budai, R.A. Zuhr, S.P. Withrow, D.O. Henderson, in: S.J. Zinkle, G.E. Lucas, R.C. Ewing, J.S. Williams (Eds.), Microstructural Processes in Irradiated Materials, Mater. Res. Soc. Symp. Proc. 540 (1999) 219.
[10] U. Kreibig, M. Vollmer, Optical Properties of Metal Clusters, Springer Series in Materials Science, Vol. 25, Springer-Verlag, Berlin, Heidelberg, 1995.

[11] M.A. van Huis, A. van Veen, H. Schut, S.W.H. Eijt, B.J. Kooi, J.Th.M. DeHosson, Rev. Adv. Mater. Sci. 4 (2003) 60.
[12] G.W. Rubloff, Phys. Rev. B 3 (1971) 285.
[13] A. van Veen, H. Schut, P.E. Mijnarends, in: P.G. Coleman (Ed.), Positron Beams and their Applications, World Scientific, Singapore, 2000, Chapter 6, p. 191.
[14] B.J. Kooi, A. van Veen, J.Th.M. De Hosson, H. Schut, A.V. Fedorov, F. Labohm, Appl. Phys. Lett. 76 (2000) 1110.
[15] W.C. Las, T.G. Stoebe, Radiat. Prot. Dosim. 8 (1984) 45.
[16] JCPDS 04-0829 (for MgO) and 04-0831 (for Zn), International Centre for Diffraction Data, 1997.